ELSEVIER

15 January 1997

Optics Communications 134 (1997) 218–222

OPTICS COMMUNICATIONS

Passive mode-locking through nonlinear polarization rotation in low-birefringence fibers

Chir-Weei Chang, Sien Chi *

Institute of Electro-Optical Engineering, National Chiao Tung University, 1001 Ta Hsueh Road, Hsinchu 300, Taiwan, ROC

Received 5 July 1996; accepted 4 September 1996

Abstract

A numerical model for the generation of ultrashort soliton pulses from erbium-doped fiber ring lasers is presented. The model is used to study the pulse dynamics of a simple cavity configuration that uses a low birefringence fiber combined with crossed polarizers. Simulations show that stable pulses with a FWHM as short as 70 fs can be generated. It is also shown that coherent coupling may enhance mode-locking in a weakly linearly birefringent fiber under optimum operation conditions, and in certain cases a period doubling bifurcation occurs due to residual linear birefringence in the fibers.

Keywords: Fiber laser; Mode-locking; Nonlinear polarization rotation

The phenomenon of nonlinear polarization rotation (NPR) in materials with Kerr type nonlinearities has led to the use of optical fibers in many applications. An important application of NPR in optical fibers has led to a new mode-locking technique for fiber ring lasers [1–6]. Picosecond pulses and sub-picosecond pulses have been generated by using a relatively long length of low-birefringence fiber operating in the multibeatlength regime [2,3]. Further improvements have been obtained by using short standard fibers [4,5]. More recently, the stretched pulse technique combined with external chirp compensation have been employed to produce high energy ultrashort pulses [6]. Previous modeling of the NPR fiber lasers was based on the coupled nonlinear Schrödinger equations without third-order dispersion, cross-Raman effects and coherent coupling [7,8]. Another kind of mode-locking that exploits polarization instability in an extremely weakly birefringent fiber was also proposed [9].

Nonlinear polarization rotation can exist in birefringent fibers [10] due to nonlinear birefringence induced phase shifting, it can also exist in isotropic media and is referred to as ellipse rotation [11]. Theoretical results from Winful [12] show that the use of low birefringence fiber provides an additional reduction in the optical power required to observe nonlinear polarization effects, and that the linear birefringence and coherent coupling that can be neglected in highly birefringent fiber [10] plays an important role in low birefringence fibers. In practice, perfectly isotropic fiber does not exist, standard fibers usually have weak linear birefringence with beat lengths L_B around 2–3 m at 1.55 μm [4]. Therefore, it is practically important to understand the details of pulse evolution in passively mode-

* Corresponding author. E-mail: schi@cc.nctu.edu.tw.

PII S0030-4018(96)00562-7

locked fiber lasers with short cavity length and weak birefringence.

This paper presents numerical results that completely describe pulse propagation in NPR fiber lasers. We have considered third-order dispersion, cross-Raman effects and coherent coupling for the ultrashort pulses. Following our earlier work on soliton pulse train amplification [13], we describe the propagation of optical pulses in erbium-doped fibers by means of a complex Lorentzian gain model that also includes the effect of gain saturation and pump absorption. The model can be used to estimate fiber length and cavity dispersion needed to generate stable short pulses with fiber ring lasers.

The coupled modified nonlinear Schrödinger equations describing femtosecond-range pulse propagation in a linearly birefringent erbium-doped fiber are [13,14]

$$
\begin{aligned}
&i\frac{\partial u}{\partial \xi} + \kappa u + i\delta\frac{\partial u}{\partial \tau} + \tfrac{1}{2}\frac{\partial^2 u}{\partial \tau^2} - id\frac{\partial^3 u}{\partial \tau^3} + |u|^2 u \\
&\quad + \tfrac{2}{3}|v|^2 u + \tfrac{1}{3}v^2 u^* \\
&\quad - \left(c_1 u\frac{\partial |u|^2}{\partial \tau} + c_2 u\frac{\partial |v|^2}{\partial \tau} + c_3 v\frac{\partial uv^*}{\partial \tau} \right) \\
&= \frac{1}{4\pi}\Gamma_0 \int_{-\infty}^{\infty} [f(\omega-\omega_0) + ig(\omega-\omega_0)] \\
&\quad \times \tilde{u}(\xi,\omega)\exp(-i\omega t)\,\mathrm{d}\omega, \qquad (1)
\end{aligned}
$$

$$
\begin{aligned}
&i\frac{\partial v}{\partial \xi} - \kappa v - i\delta\frac{\partial v}{\partial \tau} + \tfrac{1}{2}\frac{\partial^2 v}{\partial \tau^2} - id\frac{\partial^3 v}{\partial \tau^3} + |v|^2 v \\
&\quad + \tfrac{2}{3}|u|^2 v + \tfrac{1}{3}u^2 v^* \\
&\quad - \left(c_1 v\frac{\partial |v|^2}{\partial \tau} + c_2 v\frac{\partial |u|^2}{\partial \tau} + c_3 u\frac{\partial u^* v}{\partial \tau} \right) \\
&= \frac{1}{4\pi}\Gamma_0 \int_{-\infty}^{\infty} [f(\omega-\omega_0) + ig(\omega-\omega_0)] \\
&\quad \times \tilde{v}(\xi,\omega)\exp(-i\omega t)\,\mathrm{d}\omega, \qquad (2)
\end{aligned}
$$

where

$$
f(\omega-\omega_0) = \frac{-(\omega-\omega_0)T_2}{1+(\omega-\omega_0)^2 T_2^2},
$$

$$
g(\omega-\omega_0) = \frac{1}{1+(\omega-\omega_0)^2 T_2^2},
$$

$$
\Gamma_0 = \frac{T_0^2}{|\beta_2|}\sigma_s W_{ss}(\xi).
$$

In Eqs. (1) and (2), u and v are the normalized field components of the slow and fast axes, respectively (when δ is positive), 2κ is the normalized wavenumber difference, 2δ is the corresponding inverse group velocity difference, d is the normalized third-order dispersion parameter, ξ is the normalized distance, and τ is the normalized time. The terms with factors of $2/3$ represent the effect of cross-phase modulation. The effect of coherent coupling is represented by the terms with factors of $1/3$. The terms within parentheses represent the Raman effect in birefringent fiber [15]. Both the parallel and perpendicular Raman effects are retained in these equations, where $c_1 = T_R/T_0$ and $c_2 = c_3 = c_1/3$. Here $T_0 = T_{FWHM}/1.763$ is the normalized pulse width and the Raman coefficient T_R is assumed to be 3 fs in our simulations. The lineshape functions $f(\omega-\omega_0)$ and $g(\omega-\omega_0)$ represent pump-induced dispersion and gain profiles, where ω_0 is the carrier frequency of the signal pulse and T_2 is the polarization relaxation time of the pumped erbium ions. Γ_0 is the normalized peak gain coefficient and $\Gamma_0 = 0$ is the passive fiber, where β_2 is the group velocity dispersion parameter, σ_s is the emission cross section at the signal wavelength, and $W_{ss}(\xi)$ is the steady-state solution of the population inversion. Because the gain saturation can be described by the averaged power of the signal pulse train [13], the steady-state solution $W_{ss}(\xi)$ can thus be obtained by solving the three-level rate equation as follows:

$$
W_{ss}(\xi) = \frac{\tilde{I}_p(\xi) - 1}{1 + \tilde{I}_p(\xi) + \tilde{I}_s(\xi)} N_0, \qquad (3)
$$

where

$$
\tilde{I}_p = \frac{\sigma_p I_p T_1}{h\nu_p}, \quad \tilde{I}_s = \frac{2\sigma_s I_s T_1}{h\nu_s}.
$$

In Eq. (3), I_p and I_s are the intensities of the pump and signal beams, respectively; $h\nu_p$ and $h\nu_s$ are the photon energies of the pump and signal waves, respectively; σ_p is the absorption cross-section at the

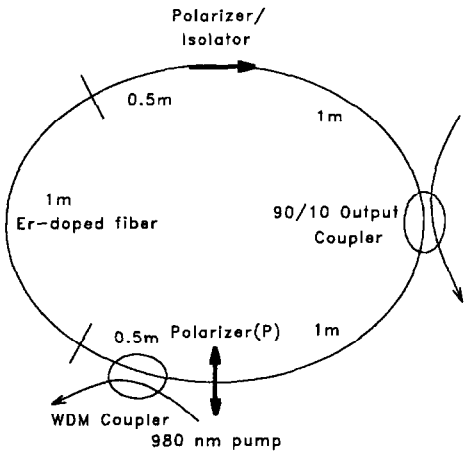

Fig. 1. Schematic diagram of the fiber laser cavity. The ring cavity of this laser incorporated 1 m of erbium-doped fiber with a total length of 4 m.

pump wavelength; N_0 is the doping density of the erbium ions, and T_1 is the relaxation time of the population inversion. Also, the equation describing the evolution of the pump intensity is

$$\frac{1}{I_p(\xi)}\frac{dI_p(\xi)}{d\xi} = -\sigma_p N_1(\xi) - \alpha_p, \tag{4}$$

where

$$N_1(\xi) = \frac{1 + 0.5\bar{I}_s(\xi)}{1 + \bar{I}_p(\xi) + \bar{I}_s(\xi)} N_0.$$

In Eq. (4), N_1 is the population density of the lower laser level in the steady state, and α_p is the intrinsic fiber loss at the pump wavelength. It is worth mentioning that the effect of pump absorption plays an important role in the amplification of ultrashort pulse trains in erbium-doped fibers, but it has usually been neglected by many authors.

Fig. 1 is a schematic diagram of the mode-locked fiber ring laser used in our simulations, and first used by Nakazawa et al. [5] to demonstrate experimentally that stable 136 fs pulses can be obtained. The ring laser consists of an erbium-doped fiber section, a polarizer (P), and a Faraday (polarization-sensitive) isolator. The Faraday isolator plays the dual role of an isolator that forces unidirectional operation and a polarizer such that light leaving the isolator is linearly polarized. In our analysis, the isolator consisted of an input polarizer and an output polarizer rotated by 45° relative to each other, and the polarization axis of the input polarizer was assumed to be orthogonal to that of the polarizer (P). It is interesting to note that the simple cavity design does not include any of the polarization controllers that are usually used in fiber ring lasers [1–4], thus the nonlinear transmission is due to the presence of linear birefringence, which changes the polarization state from linear to elliptical. However, this simple configuration can still provide information about important features of concerned mode-locked ring lasers.

The typical parameters used to solve Eqs. (1)–(4) numerically are: soliton wavelength = 1.53 μm, pump wavelength = 0.98 μm, $\beta_2 = -4$ ps^2/km, $\beta_3 = 0.1$ ps^3/km, $T_2 = 0.1$ ps, $T_1 = 11.5$ ms, $T_R = 3$ fs, $\sigma_s = 7.75 \times 10^{-25}$ m^2, $\sigma_p = 3.12 \times 10^{-25}$ m^2, $\alpha_p = 1.0$ dB/km, $N_0 = 2.39 \times 10^{19}$ ions/cm^3, which corresponds to 2300 ppm doping density, $\theta = 20°$, which is the angle between the polarization axis of the polarizer (P) and the slow axis of the fiber, and pump power = 80 mW. Eqs. (1) and (2) are solved using the split-step Fourier method assuming the initial condition

$$u(\xi = 0, \tau) = A\,\mathrm{sech}(\tau)\cos(\theta + \pi/4), \tag{5}$$

$$v(\xi = 0, \tau) = A\,\mathrm{sech}(\tau)\sin(\theta + \pi/4), \tag{6}$$

which is a linearly polarized pulse injected into the fiber right behind the output polarizer of the isolator

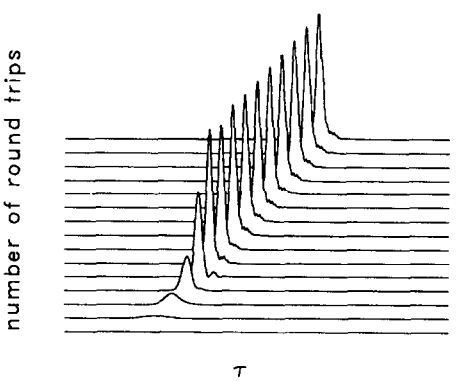

Fig. 2. Evolution of the stable output pulse (FWHM = 100 fs) with GVD = -4 ps^2/km.

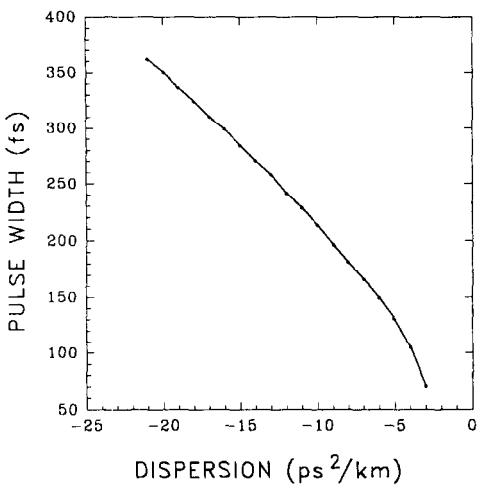

Fig. 3. Output pulse width as a function of GVD parameter.

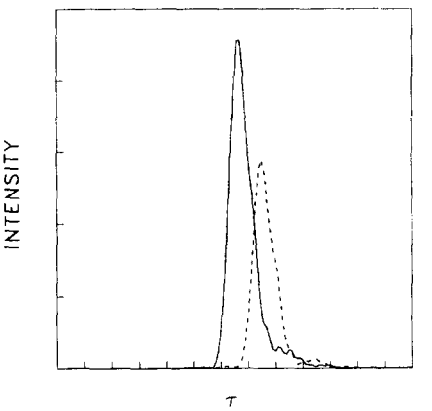

Fig. 4. Pulse shapes at the output of the ring laser after fifteen round trips with GVD $= -4$ ps^2/km. Dashed curve shows the case in which the coherence term was neglected in Eqs. (1) and (2).

at amplitude A and polarization angle $\theta + \pi/4$ with respect to the u axis. Stable operation regimes for a large range of parameters have been found, and the final steady-state pulse is independent of the amplitude and width of the initial injected pulse.

In Fig. 2, we show the evolution of an injected pulse with $A = 0.1$, width $= 1$ ps FWHM and $L_B = 2$ m through fifteen round trips. The result is a stable pulse train of width 100 fs that is free of pedestal. However we observed that the pulse shape became asymmetric with a ripple near its trailing edge, that is due to the effect of third-order dispersion. The Raman self-frequency shift does not play an important role in stable pulse regimes, which is suppressed by bandwidth-limited amplification. As can be seen, the pulse is delayed in the moving frame; i.e., the group velocity of the pulse decreased due to gain-induced dispersion, which is typical in pulse propagation through an amplifier [16]. Fig. 3 shows the output pulse width as a function of the group velocity dispersion (GVD), which is in good agreement with experimental results [17]. As GVD decreased, output pulse width decreased and the trailing edge of the pulse began rippling until the pulse broke up at GVD ~ -2 ps^2/km. The minimum stable pulse width obtained is around 70 fs for GVD ~ -3 ps^2/km, which is almost gain bandwidth limited.

In Fig. 4, it is shown that the coherent coupling term has the effect of increasing the output peak power. The reason for this can be referred to the coherent coupling between the two polarizations affecting both the amplitude and phase of the waves, and it may be exploited for enhanced mode-locking under the optimum condition. In our simulation, the approximation of high birefringence is valid for $L_B \leq 0.1$ m, where the effect of the coherence term is ignored. In order to understand the effect of residual

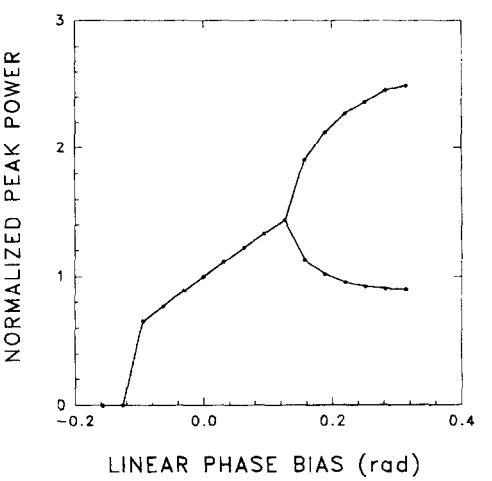

Fig. 5. Pulse peak power as a function of the linear phase bias that is due to the residual linear birefringence.

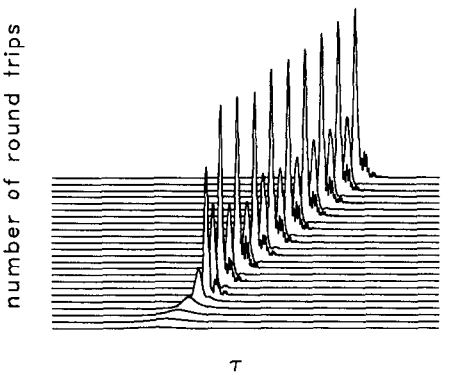

Fig. 6. Evolution of the laser pulse showing the phenomenon of period doubling with linear phase bias of $-\pi/10$.

linear birefringence, in Fig. 5 we have shown the changes in the output peak power as a function of residual linear birefringence by varying the beat length of the fiber. The output peak power was normalized with the value at null phase bias, and 2π phase bias corresponds to one beat length. We note that the NPR is strongly affected by the residual linear birefringence, and a period doubling bifurcation occurs for a certain phase bias. In Fig. 6, we have shown the phenomenon of period doubling that is the output pulses alternating between two intensity values on successive round trips, which has been observed experimentally [18–21].

In conclusion, a numerical model has been developed to study the dynamics of pulse train generation in a fiber ring laser. We have shown that stable pulses with a FWHM as short as 70 fs can be generated in an erbium-doped fiber ring laser using nonlinear polarization rotation. The influence of cavity dispersion, coherent coupling and residual intrinsic birefringence on the pulse generation were also discussed. The numerical results clearly show that a complete description of such a pulse propagation is necessary.

References

[1] V.J. Matsas, T.P. Newson and M.N. Zervas, Optics Comm. 92 (1992) 61.
[2] V.J. Matsas, T.P. Newson, D.J. Richardson and D.N. Payne, Electron. Lett. 28 (1992) 1391.
[3] D.U. Noske, N. Pandit and J.R. Taylor, Electron. Lett. 28 (1992) 2185.
[4] K. Tamura, H.A. Haus and E.P. Ippen, Electron. Lett. 28 (1992) 2226.
[5] M. Nakazawa, E. Yoshida, T. Sugawa and Y. Kimura, Electron. Lett. 29 (1993) 1327.
[6] H.A. Haus, K. Tamura, L.E. Nelson and E.P. Ippen, IEEE J. Quantum Electron. 31 (1995) 591.
[7] C.J. Chen, P.K.A. Wai and C.R. Menyuk, Optics Lett. 17 (1992) 417.
[8] V.V. Afanasjev and A.B. Grudinin, Sov. Lightwave Comm. 3 (1993) 77.
[9] P.E. Langridge, G.S. McDonald, W.J. Firth and S. Wabnitz, Optics Comm. 97 (1993) 178.
[10] R.H. Stolen, J. Botineau and A. Ashkin, Optics Lett. 7 (1982) 512.
[11] P.D. Maker, R.W. Terhune and C.M. Savage, Phys. Rev. Lett. 12 (1964) 507.
[12] H.G. Winful, Appl. Phys. Lett. 47 (1985) 213.
[13] S. Chi, C.W. Chang and S. Wen, Optics Comm. 111 (1994) 132.
[14] S.G. Evangelides Jr., L.F. Mollenauer, J.P. Gordon and N.S. Bergano, J. Lightwave Technol. 10 (1992) 28.
[15] C.R. Menyuk, M.N. Islam and J.P. Gordon, Optics Lett. 16 (1991) 566.
[16] A.E. Siegman, Lasers (University Science Books, Mill Valley, CA, 1986) p. 352.
[17] M.L. Dennis and I.N. Duling III, Appl. Phys. Lett. 62 (1993) 2911.
[18] S. Bielawski, M. Bouazaoui, D. Derozier and P. Glorieux, Phys. Rev. A 47 (1993) 3276.
[19] P. Le. Boudec, C. Jaouen, P.L. Francois, J.F. Bayon, F. Sanchez, P. Besnard and G. Stephan, Optics Lett. 18 (1993) 1890.
[20] E. Lacot, F. Stoeckel and M. Chenevier, Phys. Rev. A 49 (1994) 3997.
[21] K. Tamura, C.R. Doerr, H.A. Haus and E.P. Ippen, IEEE Photon. Technol. Lett. 6 (1994) 697.